TABLE 3 Computation Times [s] for Each Method Using a PC With an Intel® Core™ i7-2600k (3.40 GHz) Processor With 16.0 GB of RAM

Item	CM-SBR	One-Shot ISAR	Proposed Method
Computation time (T_c) [s]	489.2	3.1	19.7

shot ISAR technique [yellow dotted circle in Fig. 14(b)], the proposed method accurately describes all scatterers without the miss-detection of any major scatterer in the 2D image domain [yellow dotted circle in Fig. 14(c)]. As expected, the computation time of the proposed method ($T_c = 19.7$ s) is much faster than that of the CM-SBR ($T_c = 509.2$ s) owing to the newly devised acceleration approach using the RTM. Consequently, the results in Figure 14 and Table 3 show that the proposed scheme demonstrates considerably improved computation efficiency while retaining excellent accuracy without the spurious artifacts as well as the miss-detection of any scatterer.

4. CONCLUSION

In this paper, we proposed a new acceleration method that is suitable for accurate ISAR image generation without distortions by introducing the RTM. Owing to the RTM based on the monostatic approach, the advantage of the proposed method, while simultaneously considering the CM-SBR and the ISAR configuration is summarized as follows:

First, we generated high-resolution ISAR images using the proposed method, which led to a significant acceleration in the number of computations compared to the CM-SBR. Second, the proposed method showed excellent computation efficiency while generating ISAR images, especially at high center frequencies, because of the reduced number of small candidate rays, whereas the computation speed of the CM-SBR was much slower for the increased center frequencies. Next, the proposed method had the merit of significantly reducing the computation time for models that are composed of electrically large facets. Finally, contrary to the one-shot ISAR technique, the proposed method produced high-quality ISAR images without missing major scatterers because of the monostatic approach based on the CM-SBR, at the expense of increased computational complexity.

Consequently, the results showed that the proposed method achieved accurate ISAR images with an accurate description of scattering features within a very short period.

REFERENCES

1. C. Odzemir, Inverse synthetic aperture radar imaging with MATLAB algorithms, John Wiley & Sons, Hoboken, NJ, 2012.
2. R.O. Jernejcic, A.J. Terzuoli, and R.F. Schindel, Jr. Electromagnetic backscatter predictions using XPATCH, IEEE Antenna Propag Soc Int Sympos 1 (1994), 602–605.
3. H. Ling, R. Chou, and S.W. Lee, Shooting and bouncing rays: Calculating the RCS of an arbitrarily shaped cavity, IEEE Trans Antenna Propag 37 (1989), 194–205.
4. R. Bhalla and H. Ling, ISAR image formation using bistatic data computed from the shooting and bouncing ray technique, J Electromag Waves Appl 7 (1993), 1271–1287.
5. R. Bhalla and H. Ling, Image-domain ray-tube integration formula for the shooting and bouncing ray technique, Radio sci. 30 (1995), 1435–1446.
6. R. Bhalla and H. Ling, A fast algorithm for signature prediction and image formation using the shooting and bouncing ray technique, IEEE Trans Antenna Propag 43 (1995), 727–731.
7. D.J. Yun, J.I. Lee, K.U. Bae, K.I. Kwon, and N.H. Myung, Improvement in accuracy of ISAR image formation using the shooting and bouncing ray, IEEE Antenna Wireless Propag Lett 14 (2015), 970–973.
8. Y.B. Tao, H. Lin, and H.J. Bao, KD-tree based fast ray tracing for RCS prediction, Prog Electromagn Res 81 (2008), 329–341.
9. S.H. Suk, T.I. Seo, H.S. Park, and H.T. Kim, Multiresolution grid algorithm in the SBR and its application to the RCS calculation, Microw Opt Tech Lett 29 (2001), 394–397.
10. H.G. Park, H.T. Kim, and K.T. Kim, Beam tracing for fast RCS prediction of electrically large targets, Prog Electromagn Res M 20 (2011), 29–42.

WIDEBAND SUBSTRATE-INTEGRATED MONOPOLE ANTENNA

Nicholas P. Lawrence, Christophe Fumeaux, and Derek Abbott
School of Electrical and Electronic Engineering, The University of Adelaide, SA 5005, Australia; Corresponding author: nicholas.lawrence@adelaide.edu.au

Received 6 January 2016

ABSTRACT: *A coaxial probe fed wideband low-profile electric monopole cavity antenna with measured impedance bandwidth of 56% at a central operating frequency of 8 GHz is proposed. The antenna, based on a modified shorted square patch, effectively forms a substrate-integrated cavity with four curved radiating slots at its periphery. The concave curvature of these four radiating slots provides a magnetic current loop mode while increasing bandwidth and reducing volume of the resonator. The proposed design may be easily fed using a 50 Ω probe feed and capacitive gap, and is robust to manufacturing tolerances, as parasitic modes are not excited. The design is compatible with applications requiring a vertically polarized signal with respect to the antenna surface*. © 2016 Wiley Periodicals, Inc. Microwave Opt Technol Lett 58:1855–1857, 2016; View this article online at wileyonlinelibrary.com. DOI 10.1002/mop.29925

Key words: *antenna; polarization; monopole; planar*

1. INTRODUCTION

Low-profile monopole antennas are becoming more relevant in an increasing number of technologies in the microwave region. Specific examples include the dedicated short-range communications (DSRC) band for vehicle-to-vehicle (v2v) safety systems [1], aircraft applications [2], active [3] and passive [4] sensor technologies, and unattended ground sensors (UGSs) [5]. For each of these applications, an antenna backed by a ground plane that can be integrated into an RF substrate appears very attractive. With such an antenna vertically mounted, one desired feature is an omnidirectional radiation pattern, making it useful for terrestrial applications, non-line-of-sight (NLoS) conditions, and situations where transceiver modules may be deployed randomly. A gain profile with maximum in or close to the substrate plane is possible; this being achieved by either a standalone device, or by mounting on a large metallic surface. Design architecture is varied, and includes a miniaturized cavity-backed composite slot loop antenna (CBCSLA) [6], and a multiple-element monopole design [7], as well as low-profile resonant cavities, with fringing fields from thin apertures forming equivalent magnetic currents [8].

Generally, low-profile monopole antennas can be split into two geometries: square [9–11] and circular [12–16] cavities. More complex cross and conical geometries [17] may be employed to increase bandwidth. Circular designs tend to

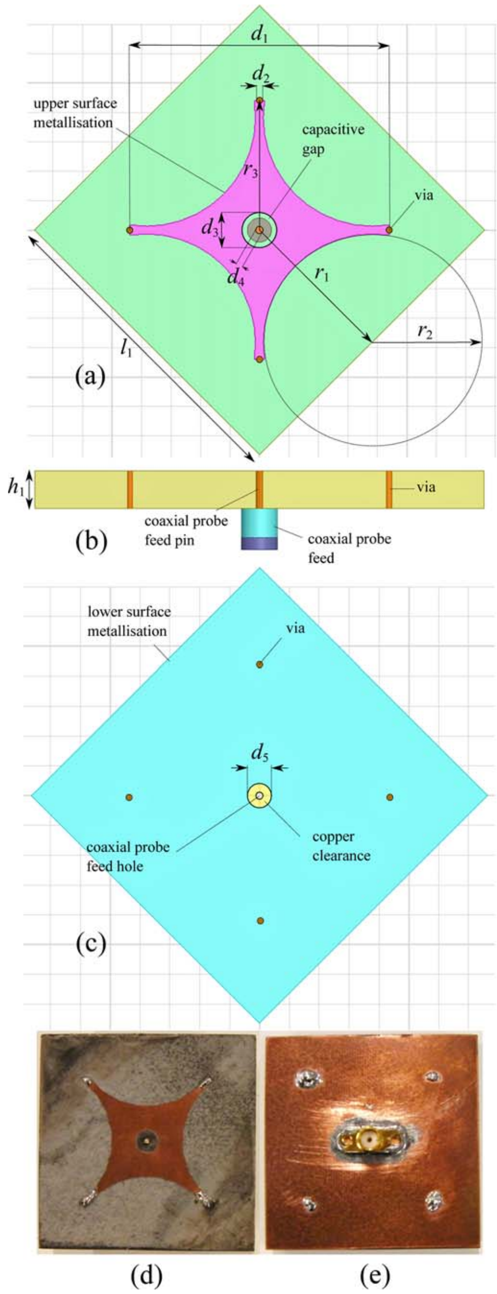

Figure 1 The antenna design operates as a magnetic current loop via 4 concavely curved radiating slots, providing a symmetric radiation pattern through excitation of a magnetic current loop mode. Views shown are: (a) top view, (b) front view, (c) bottom view (with coaxial probe feed connection removed), (d) manufactured topside, (e) manufactured backside. [Color figure can be viewed in the online issue, which is available at wileyonlinelibrary.com]

resonate with cylindrical TM_{01} and TM_{02} modes while square patches tend to resonate with TM_{11} and higher-order modes. Resonator height is largely influenced by the choice of cavity medium. Free-space cavities generally lead to higher resonant frequencies for a given cavity size, and are often voluminous. Higher permittivity designs suffer from higher losses and decreased bandwidth.

For v2v and aircraft applications, the extended ground plane offered to the monopole in the form of large metallic outer surface renders the use of such an antenna an extremely attractive option. Such a surface offers the possibility of generating an omnidirectional radiation pattern with a maximum gain near the substrate plane. The ground plane shape influences the antenna radiation pattern.

For UGS and active and passive sensor applications, the stand-alone device may provide vertical polarization with a radiation pattern that remains omnidirectional in a narrow bandwidth.

In this paper, we propose an easily manufacturable low-profile magnetic loop monopole antenna design, and demon strate how a simple modification of the patch geometry, namely the Introduction of concave curved edges, can significantly increase the operational bandwidth.

2. DESIGN

Figure 1 illustrates the proposed antenna design, with dimensional information given in Table 1. The design is based on a Rogers Duroid® 5880 substrate with relative permittivity ϵ_r of 2.2, loss tangent $\delta = 0.0009$, and is cladded with 17μm of copper on either side. Its geometry consists of an evolution of a square patch shorted at its corners, where the four radiating cavities are modified to curved concave shapes. This effectively forms a substrate-integrated cavity radiating as a magnetic current loop. This can be understood from the equivalence of a small constant magnetic current loop and an electric dipole, which is the dual case of a small loop of constant electric current being equivalent to a magnetic dipole.

At the centre of the upper surface, the annular capacitive gap between the coaxial probe feed centre pin and the upper surface concave patch compensates the inductive nature of the cavity coaxial feed, providing control of impedance and input reflection coefficient of the antenna [11].

The substrate height h_1 corresponds to a guided wavelength of $\lambda/5$ at 5.8 GHz, the lowest frequency of operation. While this can be considered high by some measures, this height enables the antenna bandwidth to significantly increase compared to a previous design using a substrate height of 3.2 mm [11]. This dependence of bandwidth on resonator height is consistent with observations of related microstrip patch antenna structures.

3. RESULTS

Figure 2 shows the simulated and measured input reflection coefficient S_{11} of the optimized geometry. The measured impedance bandwidth is 56%, as per an input reflection coefficient criteria of $|S_{11}| \leq -10$ dB with respect to a 50 Ω characteristic. Prior work has demonstrated a narrow bandwidth of 2.1% at a design frequency of 5.9 GHz for a design of comparable ground plane area, due to a reduced substrate height [11]. Figure 2 illustrates the bandwidth improvement that can be achieved by doubling the substrate height, and thus the monopole cavity height.

TABLE 1 Antenna Dimensions

Reference	Dimension
l_1 (antenna side length)	54 mm
h_1 (antenna side height)	6.35 mm
d_1 (circular copper diameter)	44.00 mm ⊘
r_1 (circular cutout centre point radius)	027.00mm
r_2 (circular cutout radius)	18.50 mm
r_3 (radial via distance)	22.00 mm
d_2 (via diameter)	1.05 mm ⊘
d_3 (upper surface copper clearance diameter)	5.97 mm ⊘
d_4 (pin diameter)	1.27 mm ⊘
d_5 (coaxial feed copper clearance diameter)	4.1 mm ⊘

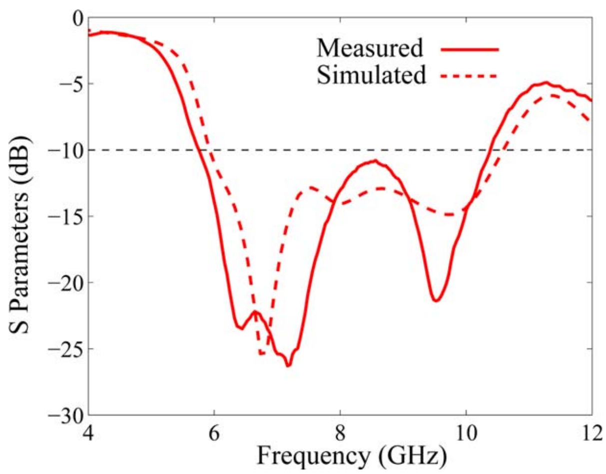

Figure 2 Reflection coefficient of the proposed antenna. The measured impedance bandwidth of the antenna, defined by an input reflection coefficient $|S_{11}| \leq -10$ dB, is from 5.8 GHz to 10.3 GHz. The measured shift down in frequency has been previously observed with a similar structure [11]. Complex impedance matching results in the observed divergence between simulation and measurement at 6.3–7.2 GHz, and at 9.3 GHz. [Color figure can be viewed in the online issue, which is available at wileyonlinelibrary.com]

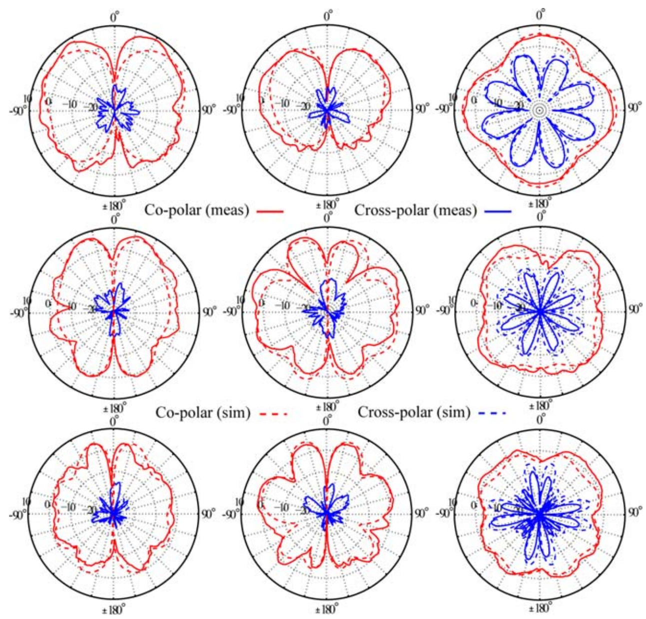

Figure 3 Antenna realised gain patterns at 5.9 GHz (top row), 8 GHz (middle row), and 10.3 GHz (bottom row). Sectional cuts of $\phi_0°$ (left column), $\phi_{45°}$ (middle column), and $\theta_0°$ (right column) are shown. [Color figure can be viewed in the online issue, which is available at wileyonlinelibrary.com]

Simulated and measured antenna realized gain patterns are illustrated in Figure 3 at the low, mid- and upper bandwidth frequencies. As can be seen, patterns are symmetric and quasi-omnidirectional; consistent with similar reported structures. An extended ground plane, as in a v2v system, would provide a more omnidirectional pattern with a reduced maximum gain parallel to the planar antenna surface.

4. CONCLUSION

We have presented a wideband low-profile monopole cavity substrate-integrated antenna, centred at 8 GHz, and with a 56% measured impedance bandwidth. Realized gain patterns illustrated at lower, mid- and upper bandwidth frequencies demonstrate vertical polarization, as seen by a broadside null, and are symmetric and quasi-omnidirectional about an axis perpendicular to the antenna surface. The design proposes fewer components than prior work, suggesting less reliance on manufacturing tolerance.

The antenna may offer a more omnidirectional radiation pattern, with maximum gain near the substrate plane, when mounted onto a large metallic surface. As such, the design is particularly well suited to v2v systems and aircraft applications.

REFERENCES

1. S. Biswas, R. Tatchikou, and F. Dion, Vehicle-to-vehicle wireless communication protocols for enhancing highway traffic safety, IEEE Commun Mag 44 (2006), 74–82.
2. K. Sampigethaya, R. Poovendran, S. Shetty, T. Davis, and C. Royalty, Future e-enabled aircraft communications and security: The next 20 years and beyond, Proc IEEE 99 (2011), 2040–2055.
3. G. Marrocco, L. Mattioni, and C. Calabrese, Multiport sensor RFIDs for wireless passive sensing of objects–basic theory and early results, IEEE Trans Antenna Propag 56 (2008), 2691–2702.
4. C. Mandel, B. Kubina, M. Schubler, and R. Jakoby, Passive chipless wireless sensor for two-dimensional displacement measurement, in *41st European Microwave Conference (EuMC)*, 2011, pp. 79–82.
5. J. Nemeroff, L. Garcia, D. Hampel, and S. DiPierro, Application of sensor network communications, in IEEE Military Communications Conference, 2001. MILCOM 2001. Communications for Network-Centric Operations: Creating the Information Force, vol. 1, 2001, pp. 336–341.
6. H. Wonbin and K. Sarabandi, Low profile miniaturized planar antenna with omnidirectional vertically polarized radiation, IEEE Trans Antenna Propag 56 (2008), 1533–1540.
7. H. Wonbin and K. Sarabandi, Low-profile, multi-element, miniaturized monopole antenna, IEEE Trans Antenna Propag 57 (2009), 72–80.
8. S.J. Lin and J.S. Row, Monopolar patch antenna with dual-band and wideband operations, IEEE Trans Antenna Propag 56 (2008), 900–903.
9. J.S. Row and S.H. Chen, Wideband monopolar square-ring patch antenna, IEEE Trans Antenna Propag 5 (2006), 1335–1339.
10. S. Abadi and N. Behdad, An electrically small, vertically polarized ultrawideband antenna with monopole-like radiation characteristics, IEEE Antenna Wireless Propag Lett 1 (2014), 742–745.
11. T. Kaufmann and C. Fumeaux, Low-profile magnetic loop monopole antenna based on a square substrate-integrated cavity, Int J Antenna Propag (2015), Article ID 694385.
12. A. Al-Zoubi, F. Yang, and A. Kishk, A broadband center-fed circular patch-ring antenna with a monopole like radiation pattern, IEEE Trans Antenna Propag 57 (2009), 789–792.
13. L. Economou and R. Langley, Patch antenna equivalent to simple monopole, Electron Lett 33 (1997), 727–729.
14. J. Liu, Q. Xue, H. Wong, H.W. Lai, and Y. Long, Design and analysis of a low-profile and broadband microstrip monopolar patch antenna, IEEE Trans Antenna Propag 61 (2013), 11–18.
15. H. Nakano, H. Iwaoka, K. Morishita, and J. Yamauchi, A wideband low-profile antenna composed of a conducting body of revolution and a shorted parasitic ring, IEEE Trans Antenna Propag 56 (2008), 1187–1192.
16. J. Liu, S. Zheng, Y. Li, and Y. Long, Broadband monopolar microstrip patch antenna with shorting vias and coupled ring, IEEE Antenna Wireless Propag Lett 13 (2014), 39–42.
17. M. Koohestani, J.F. Zürcher, A. Moreira, and A. Skrivervik, A novel, low-profile, vertically-polarized UWB antenna for WBAN, IEEE Trans Antenna Propag 62 (2014), 1888–1894.